

ARTICLE

Automated lung cancer detection using artificial intelligence techniques

Naziya Anjum*, and Mohd Haroon

Department of Computer Science and Engineering, Faculty of Engineering & Information Technology, Integral University, Lucknow, Uttar Pradesh, India

Abstract

Lung cancer is a leading cause of cancer-related mortality due to delayed diagnosis and limitations of conventional screening methods. This study presents an artificial neural network-based computer-aided diagnosis system for automated lung cancer detection using computed tomography scans. The proposed methodology integrates advanced digital image processing techniques with machine learning-based classification to improve diagnostic accuracy and reliability. The framework consists of multiple stages. Initially, computed tomography images are preprocessed using a two-dimensional median filter to suppress noise while preserving structural boundaries. Morphological operations and contrast enhancement techniques are applied, followed by adaptive thresholding to segment lung regions. A seeded region growing technique is then employed to identify suspicious regions and extract relevant image segments. From these segments, 25 texture features are computed using the gray level co-occurrence matrix, capturing statistical properties such as contrast, correlation, entropy, homogeneity, and energy. Two artificial neural network classifiers, namely the back propagation neural network and the radial basis function neural network, are trained using these features. A dataset of 500 computed tomography images, including both cancerous and non-cancerous cases, is used for performance evaluation. Experimental results demonstrate that both models achieve high classification accuracy, sensitivity, and specificity, while the radial basis function neural network consistently outperforms the back propagation neural network, achieving a maximum accuracy of 94%. These findings highlight the effectiveness of the proposed system as a reliable, non-invasive, and computationally efficient tool for early lung cancer detection, with potential applicability to other medical imaging domains.

***Corresponding author:**Naziya Anjum
(syednazia@student.iul.ac.in)

Citation: Anjum N., Haroon M. (2026). Automated lung cancer detection using artificial intelligence techniques. *Int J Systematic Innovation*, 10(3): 026090017. [https://doi.org/10.6977/IJoSI.202606_10\(3\).0002](https://doi.org/10.6977/IJoSI.202606_10(3).0002)

Received: February 28, 2026**Revised:** April 12, 2026**Accepted:** April 28, 2026**Published online:** June 15, 2026

Copyright: © 2026 Author(s). This is an Open-Access article distributed under the terms of the Creative Commons Attribution License, permitting distribution, and reproduction in any medium, provided the original work is properly cited.

Publisher's Note: AccScience Publishing remains neutral with regard to jurisdictional claims in published maps and institutional affiliations.

Keywords: Artificial neural network; Lung cancer detection; Computer-aided diagnosis; Gray level co-occurrence matrix; Back propagation neural network; Radial basis function neural network

1. Introduction

Lung cancer is a global health issue, causing the death of 1.8 million people annually (World Health Organization, 2026). Although lung cancer treatment has improved, survival is still poor, seldom surpassing five years. Given that early-stage lung cancer includes low-grade, broad, or non-specific symptoms that delay clinical treatment,

late identification is a major risk. Improving survival, treatment planning, and mortality requires rapid and effective detection. Low-dose computed tomography (LDCT) is used for early lung cancer screening because it is more sensitive than chest radiography (Verma *et al.*, 2025). LDCT can detect small pulmonary nodules, but its high false-positive rate causes unnecessary follow-up therapies, intrusive biopsies, higher healthcare expenditures, and emotional anguish (Mathew *et al.*, 2025). Smoking history, genetics, work-related exposures, and environmental factors are ignored in current screening guidelines. This slows screening and strains healthcare systems (Y. Liu *et al.*, 2024). Artificial intelligence (AI) is revolutionary and can improve diagnostics. Using sophisticated computer models and data-driven learning, AI-based systems can interpret complex, high-dimensional medical data more effectively than humans. Radiomics and AI-based machine learning can detect trends in LDCT images that radiologists miss. With novel non-invasive diagnostic methods such as liquid biopsy (specifically circulating tumor DNA and exosomal RNA testing) and clinical data (demographic, lifestyle, and comorbidity), AI can assist with more personalized and comprehensive diagnostics (Alakwaa *et al.*, 2017). Most AI technologies are black boxes, making management difficult and leading clinicians to distrust them. Many models trained on heterogeneous patient populations are trained on homogeneous or institution-specific data, leading to bias, fairness, and generalizability issues. Risk profile-adaptive screening treatments that improve screening schedules and diagnostic cut points are similarly understudied (Anthimopoulos *et al.*, 2016). AI improvements and increasing access to high-resolution CT imaging have increased lung cancer diagnosis. CT images show lung structures in cross-section, allowing detection of small nodules and early disease changes (Ardila *et al.*, 2019). The rising amount and complexity of CT data load increase radiologists' cognitive and operational stress, making manual interpretation time-consuming and variable. This has boosted the use of computer-aided diagnosis (CAD) systems to help clinicians improve diagnostic precision, consistency, and efficiency (Bhandary *et al.*, 2020).

The contemporary CAD systems reduce noise, enhance contrast, and transform the structure of medical images through digital image processing. Preprocessing and partitioning of lung and suspected tumor regions should be performed properly, as these regions are designated as regions of interest for later analysis (Chen *et al.*, 2025). Spatial continuity and intensity uniformity methods of regional segmentation have distinguished the aberrant tissue of lung CT very well. The machine learning models require feature extraction after segmentation to transform visual input into discriminative numerical information.

Medical imaging relies on texture as an indicator of the spatial interactions and heterogeneity of malignant tissue (Chen *et al.*, 2025). The old statistical texture analysis method, the gray level co-occurrence matrix (GLCM), extracts properties such as contrast, correlation, entropy, homogeneity, and energy, which have been widely studied in cancer detection. Pattern recognition, nonlinear classification, and decision-making are enhanced by brain-inspired artificial neural networks (ANNs) (Duan *et al.*, 2025). They are particularly well-suited for medical diagnostics, as they can identify complex connections in high-dimensional, noisy data. Back propagation neural networks (BPNNs) and radial basis function neural networks (RBFNNs) are popular ANN architectures because they complement one another in terms of supervised learning, convergence, and generalization (Y. Wang *et al.*, 2026). For these reasons, recent studies have developed an ANN-based CAD system to identify lung cancer in CT images (Rajagopalan & Babu, 2020). Image preprocessing, region-based segmentation, GLCM texture feature selection, and ANN-based classification are used to differentiate malignant from non-cancerous lung images. BPNN and RBFNN classifiers are compared in terms of accuracy, sensitivity, specificity, and correctness with clinical CT data (Gao *et al.*, 2024). Our objective is to develop a dependable, non-invasive, and computationally efficient diagnostic model to help radiologists identify lung cancer early and apply the model to other malignancies, imaging methods, and enhanced learning methods in future research (Hendrix *et al.*, 2023).

1.1. Problem statement

The current methods of lung cancer diagnosis using CT have several limitations. High-resolution CT scans are difficult to interpret manually because they require substantial time, are cognitively taxing, and are prone to subjectivity. Although methods that use deep learning have demonstrated promising performance, in many cases, they require large-scale annotated datasets, substantial computational resources, and are not transparent in their decision-making process. By contrast, most classical machine learning methods either rely on poor feature representations or fail to adequately assess clinically meaningful performance metrics, such as sensitivity and specificity. Moreover, comparisons of various ANN structures are underrepresented within a single experimental design. These loopholes encourage the development of a powerful, understandable, and computationally effective CAD mechanism for detecting lung cancer.

1.2. Motivation of the study

This work was motivated by a clinical need for a non-invasive, reliable, and scalable diagnostic instrument to detect early lung cancer using readily available CT imaging. Texture heterogeneity is a well-known predictor of harmful tissue development, and quantitative statistics of texture descriptors can provide meaningful quantitative images of these changes. Since ANNs can estimate nonlinear relationships among features in high-dimensional feature spaces, they are well-suited for medical image classification. The combination of efficient image preprocessing, region-based segmentation, handcrafted texture features, and ANN-based classification can be exploited to develop a CAD framework that balances diagnostic accuracy, interpretability, and calculability and can be adapted to the real-world clinical environment.

1.3. Novelty of the work

The proposed study is new in its methodical and comparative ANN-based CAD framework that combines classical image processing with discriminative texture analysis and neural network classification. In contrast to end-to-end deep learning models, the presented model focuses on controlled feature extraction using GLCM descriptors, enabling a more comprehensive interpretation of texture-based patterns of malignancy. Additionally, this study provides a fair and comprehensive comparison between BPNN and RBFNN under the same preprocessing, feature extraction, and evaluation conditions. The framework is tested on multi-institutional clinical CT data, and performance is measured using clinically relevant metrics, thereby boosting its translational applicability.

1.4. Key contributions

While previous studies have explored combinations of image preprocessing, texture feature extraction, and neural network-based classification, the primary limitations are insufficient experimental rigor, limited reproducibility, and limited interpretability. This work addresses these gaps by focusing on (i) a reproducible radiomics pipeline with clearly defined acquisition and preprocessing steps, (ii) rigorous evaluation using patient-level data partitioning to avoid data leakage, and (iii) incorporation of explainable AI techniques to interpret model predictions. Thus, the contribution of this study lies not in proposing a new algorithmic paradigm but in providing a robust, transparent, and clinically interpretable framework for lung cancer detection. Although deep learning-based approaches such as convolutional neural networks (CNNs) (Aslan, 2025) and three-dimensional CNNs have demonstrated high performance, their reliance on large datasets and computational complexity motivates the exploration of

lightweight, interpretable alternatives. To enhance model transparency and clinical trust, explainable AI techniques are incorporated to interpret the contribution of texture features toward classification decisions.

The most important works of this work could be summed up as follows:

- (i) Creation of a robust CAD system to detect lung cancer through CT images by incorporating preprocessing, segmentation, texture features mining, and ANN classification.
- (ii) Application of an effective region-of-interest (ROI) extraction plan with seeded region growing to precisely localize suspicious lung regions.
- (iii) Selection of 25 discriminative GLCM-based texture features to represent the spatial and statistical heterogeneity of lung tissues.
- (iv) Comparative analysis of BPNN and RBFNN classifiers on a common experimental protocol, with their strengths and weaknesses in diagnosis.
- (v) Widespread performance evaluation based on accuracy, sensitivity, specificity, correctness, and quality ratio on a clinically verified dataset of 500 CT images.

2. Literature review

Early and correct diagnosis of cancer of the lungs is a known research topic because of its impact on patient survival and prognosis (Hussein *et al.*, 2017). With increased access to medical imaging data and computational resources, automated diagnostic systems could improve radiological examinations and reduce diagnostic variability (Gaikwad *et al.*, 2026). The literature on lung cancer detection can be divided into three categories: image-processing-based, machine learning-based, and hybrid CAD systems (Jeyakumar *et al.*, 2026). An automated lung cancer diagnosis used classical image processing techniques to improve CT scans to identify suspicious nodules in the lungs (Armato *et al.*, 2001). Median filtering, histogram equalization, and morphological processes were also notable preprocessing techniques for reducing noise and enhancing image contrast (Thanoon *et al.*, 2023). Thresholding, region growth, and edge-based techniques were used to segment lung regions and potential nodules (Zheng & Lei, 2018). These methods have been successful in controlled scenarios but have failed in most situations due to imaging artifacts, parameter selection, and inter-patient variation (Jiang *et al.*, 2018).

Scientists applied machine learning algorithms to categorize them, outperforming rule-based techniques. They mainly used feature-based techniques, with handcrafted features in dotted areas, to learn classifiers

(Pehrson *et al.*, 2019). They are important because texture-based features can model the heterogeneity associated with the development of malignant tissue. The statistical texture measures, which were common and promising for differentiating benign and malignant lung tissues, were the GLCM-based measures of contrast, correlation, entropy, and homogeneity (H. Wu *et al.*, 2013). One of the oldest and most effective machine learning models for classifying lung cancer is the ANN. They can model nonlinear associations and learn complex patterns from data, making them well-suited for medical image processing. Many studies employed feed-forward neural networks and BPNNs using the texture, shape, and intensity of CT images (X. Wang *et al.*, 2019). These models were found to perform better than earlier statistical classifiers, but their slow rates of convergence, sensitivity to initial weights, and tendency to overfit rendered them inapplicable for small datasets (Abiyev & Ma'aitah, 2018).

Radial basis function neural networks were subsequently studied as an alternative ANN architecture to correct the shortfalls of BPNNs. RBFNNs use localized activation functions, which train them faster and generalize to complex decision boundaries (Yang *et al.*, 2022). RBFNNs are superior and more sensitive at detecting lung cancer than BPNNs, particularly when the features are nonlinearly separable. Studies highlighted the need to select the appropriate ANN design based on the data type and the depth of categorization (Selvakumari & Deepa, 2016). As with ANN-based classifiers, X. Wang *et al.* (2019) tested k-nearest neighbors, support vector machines, and decision trees. Support vector machines performed well in high-dimensional feature spaces, but kernel and parameter tuning were especially important. Such classifiers lacked the adaptive learning ability of neural networks; hence, they were unable to adapt to diverse clinical data. ANN-based models were popular because of their versatility and power (J. Liu *et al.*, 2024; Ma *et al.*, 2025).

Hybrid CAD systems that combine digital image processing with handcrafted feature extraction and ANN-based classification continue to trade off performance, interpretability, and computational efficiency. These systems, unlike end-to-end deep learning models, can actively control feature selection, simplify training, and provide deeper insight into the decision-making process. Despite the achievements, there are gaps in these models (Bairagi *et al.*, 2026). The use of homogeneous or institution-specific data is common in the literature, which limits its applicability to other populations. Additionally, comparisons of ANN architectures under similar experimental conditions have received inadequate attention. The concept of performance appraisals is often

centered on precision rather than on sensitivity, specificity, and accuracy, which are clinically relevant. The current research is based on a structured ANN-based CAD system with robust image preprocessing, region-based segmentation, GLCM-based texture features extraction, and BPNN and RBFNN classifiers. The proposed approach would apply clinically derived CT images to performance assessment, using features and systematic approaches to enable reliable, interpretable, and efficient real-world lung cancer diagnosis (Messay *et al.*, 2010). Table 1 presents an organized overview of prior studies, highlighting their methodologies, key findings, and the gaps that underpin the current work.

3. Methodology

3.1. Proposed framework

The CAD system is based on preprocessed CT images, ROI-localized regions, extracted texture features, and finally recognized by an ANN. Figure 1 demonstrates a powerful, scalable, extensible, modular pipeline paradigm that optimizes all the steps without altering the workflow. Clinical lung CT images were obtained via supervised learning and classified as malignant or non-cancerous. The images were then received by the system. Pulmonary components were disaggregated, and images were preprocessed to enhance quality and facilitate their analysis. A two-dimensional median filter removed sporadic noise while preserving edge data. Images were enhanced to be contrasty and vibrant, emphasizing the issue. Using erosion and dilatation, fine structures and structural boundaries were sharpened. Finally, methods based on thresholding segmented the lungs to differentiate anatomically significant parts, which were further analyzed. ROI extraction was used to detect worrisome tumor areas after preprocessing. The localization of abnormal tissue patches was performed using seeded region growth based on spatial connectivity and pixel intensity similarity. This aided in detecting candidate tumor locations and reduced interference from normal tissue. The GLCM was used to extract texture features of the extracted ROIs. The GLCM yielded the second-order statistical texture, which displays the intensities of spatial pixels. The heterogeneity of malignant tissues was characterized using 25 discriminative textural features, including contrast, correlation, entropy, homogeneity, and dissimilarity. These features provided a compact representation for tissue classification. ANN models were subsequently evaluated for classification performance. The BPNN differs from the RBFNN in its learning approach: BPNN employs supervised learning with gradient-based optimization to minimize classification error through iterative weight

Table 1. Comprehensive comparison of existing studies

Study	Dataset/setting	Task	Method	Core model/features	Reported metric (High level)	Limitations/gaps
Hendrix <i>et al.</i> (2023)	Clinically indicated CT	Benign vs. malignant nodule detection/diagnosis	Deep learning	AI system for nodule detection + diagnosis	High diagnostic performance in clinical CT	Requires careful external validation; workflow + calibration issues
Saied <i>et al.</i> (2023)	CT nodule datasets	Nodule malignancy classification	Radiomics/ML	Radiomics-based feature engineering + ML	Competitive performance reported	Feature stability and multi-center generalization remain challenging
Gao <i>et al.</i> (2024)	CT nodule benchmarks	Nodule detection & segmentation comparison	Deep learning	Comparative evaluation of DL detection/segmentation	Highlights methodological bias; performance varies by setup	Lack of standardized evaluation across studies
J. Liu <i>et al.</i> (2024)	Synthetic LDCT + radiomics	Nodule malignancy classification	Radiomics/ML	Radiomics model trained with synthetic LDCT	Feasibility shown; improved robustness claimed	Synthetic-to-real domain shift needs deeper validation
C. Wang <i>et al.</i> (2024)	CT nodules	Reliable + explainable nodule diagnosis	Explainable AI/CAD	Reliability- and explainability-oriented modeling	Improved trustworthiness focus	Explainability may trade off with accuracy; clinical validation is needed
Duan <i>et al.</i> (2025)	LDCT	Early lung cancer detection	Deep learning	Hybrid DL with 3D segmentation + classification blocks	Strong early-detection performance reported	Annotation burden; compute + deployment complexity
Yang <i>et al.</i> (2022)	LDCT (alternative training set)	Label-free risk prediction	Deep learning	Parenchyma-driven DL risk model	Effective risk prediction without large nodules	Clinical acceptance requires calibration, thresholds, and prospective studies
Ma <i>et al.</i> (2025)	Review (clinical CAD synthesis)	CAD progress + bedside integration	Review	Multimodal fusion, interpretability, privacy-preserving learning	Summarizes AUC/FP-scan ranges across systems	Points to translation gaps: fairness, generalization, interpretability
Javed <i>et al.</i> (2024)	Review (2015–2024)	DL-based lung cancer detection/classification	Review	CNN-focused DL synthesis	Broad evidence consolidation	Notes heterogeneity of datasets/metrics; limited clinical validation
Abdullahi <i>et al.</i> (2025)	Systematic review (PRISMA)	DL for lung cancer via CT	Review	1,448-article synthesis; clinical implications	Consolidates trends + challenges	Emphasizes generalizability, data variability, and integration barriers
Proposed work	500 CT images (multi-institute, India)	Malignant vs. non-cancerous classification	Hybrid CAD + ANN	Median filtering + morphology + thresholding + SRG ROI + 25 GLCM features + BPNN vs RBFNN	RBFNN is superior in the overall experiments	Future: external multi-center validation, explainable AI layer, broader radiomics feature sets

Abbreviations: 3D: Three-dimensional; AI: Artificial intelligence; ANN: Artificial neural network; BPNN: Back propagation neural network; CAD: Computer-aided diagnosis; CNN: Convolutional neural network; CT: Computed tomography; DL: Deep learning; GLCM: Gray level co-occurrence matrix; LDCT: Low-dose computer tomography; ML: Machine learning; RBFNNs: Radial basis function neural networks; ROI: Region-of-interest.

adjustment, whereas RBFNN uses localized radial basis activation functions, enabling faster convergence and improved modeling. Classifiers were used to classify lung images as malignant or non-malignant. The analytics of the proposed framework rely on clinically meaningful measures to define true positives, true negatives, false positives, and false negatives. Diagnostic reliability and clinical usefulness are important measures of assessment based on accuracy, sensitivity, and specificity.

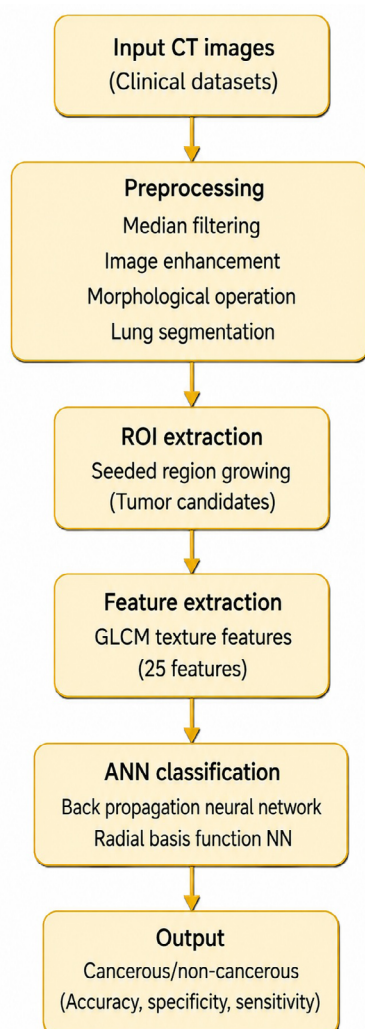


Figure 1. Proposed ANN-based computer-aided diagnosis framework for lung cancer detection using computed tomography (CT) images
Abbreviations: ANN: Artificial neural network; GLCM: Gray level co-occurrence matrix; ROI: Region-of-interest.

3.2. Dataset description

An experimental analysis of 500 lung CT scans from various clinical origins was conducted to achieve diversity

and realism. The sample contains supervised classification (malignant and non-cancerous cases). A total of 300 CT images from PGI Chandigarh, India, comprising 120 malignant and 180 non-cancerous samples, and 200 CT images from the medical college in Srinagar, India, consisting of 155 carcinogenic and 45 non-cancerous samples, were included. The sample comprised 275 cancerous and 225 benign CT scans. All pictures were assessed and classified clinically to train and evaluate. To ensure a realistic and unbiased evaluation of the proposed model, the dataset was partitioned at the patient level rather than at the image level. All CT images from a single patient were grouped and assigned exclusively to either the training or the testing subset. This prevents any overlap of patient-specific characteristics between training and testing data. Such a patient-wise splitting strategy is critical in medical imaging studies, as image-level splitting can lead to data leakage, where images from the same patient appear in both the training and test sets (Ashames *et al.*, 2024). This can artificially inflate performance metrics by causing the model to learn patient-specific patterns rather than generalizable disease characteristics. By enforcing strict patient-level separation, the proposed framework ensures that the reported performance reflects true generalization capability on unseen patients. The dataset was split using a stratified hold-out approach, with 80% of patients allocated to the training set and 20% to the test set. This strategy preserves class distribution while preventing information leakage that could otherwise artificially inflate performance. In addition, five-fold cross-validation was performed on the training set to optimize model parameters and assess robustness. This approach ensures reliable generalization and prevents overfitting.

To ensure reproducibility and consistency of radiomic feature extraction, detailed CT acquisition parameters were considered. The dataset consists of 500 lung CT images collected from two Indian hospitals under standardized clinical protocols. The CT scans were acquired using multi-detector CT systems with the following parameters: slice thickness ranging from 1 mm to 2.5 mm, tube voltage of 120 kVp, and tube current ranging from 100–250 mA, depending on patient-specific adjustments. Images were reconstructed using a standard lung kernel to preserve high-frequency texture details, which are essential for radiomic analysis. The in-plane resolution was maintained at 0.5–0.8 mm, and all images were stored in DICOM format with 12- or 16-bit grayscale depth. Prior to feature extraction, images were resampled to a uniform spatial resolution to minimize inter-scanner variability. These acquisition and reconstruction parameters are critical as GLCM-based texture features are highly sensitive to

spatial resolution, noise characteristics, and reconstruction algorithms, as shown in [Table 2](#).

Table 2. Computed tomography acquisition parameters

Parameter	Value
Modality	Multi-detector computed tomography
Slice thickness	1–2.5 mm
Tube voltage	120 kVp
Tube current	100–250 mA
Reconstruction kernel	Standard lung kernel
In-plane resolution	0.5–0.8 mm
Image format	DICOM
Bit depth	12–16 bit

3.3. Training and testing strategy

The dataset, consisting of 500 CT images, was divided into training and testing subsets using a stratified hold-out validation strategy at the patient level to preserve class distribution across malignant and non-cancerous cases. Specifically, all images for a given patient were assigned exclusively to either the training or the testing set, ensuring no patient overlap between the sets. Specifically, 80% of the data (400 images) was used for training, while the remaining 20% (100 images) was reserved for independent testing.

To ensure robustness and reduce bias from random partitioning, a five-fold cross-validation procedure was also performed on the training set. In this approach, the training data was partitioned into five equal subsets, with four used for model training and one for validation in each iteration. The process was repeated five times, such that each subset served as validation exactly once. The final model performance was computed by averaging the results across all folds. This combined strategy of hold-out testing and cross-validation ensures reliable estimation of model generalization performance while minimizing variance in evaluation. During cross-validation, patient-wise grouping was maintained to ensure that images from the same patient did not appear in both training and validation folds within any iteration.

3.4. Preprocessing configuration

To ensure the integrity of the experimental evaluation, special care was taken to avoid data leakage during model development. Data leakage occurs when information from the test set is unintentionally used during training, leading to overly optimistic performance estimates. In the present

research, the data were split before any preprocessing or feature extraction. Separation at the patient level was also rigorously enforced to ensure that no subject-specific imaging properties overlapped across the training, validation, and test sets, thereby removing a significant source of data leakage in medical imaging research. Filtering, segmentation, region-of-interest extraction, and GLCM feature computation were conducted separately on the training and testing sets. This is to ensure that the test set did not contain any information that affected the training process. Moreover, feature extraction and model training were performed within each fold during cross-validation, thereby avoiding cross-fold leakage. There was no overlap of samples in the training, validation, and testing subsets. Such precautions ensure that the reported performance measures reflect the true generalization ability of the proposed framework and are not influenced by accidental information leakage. All CT images were resampled to a uniform voxel spacing, and intensity standardization was applied to ensure consistency across images acquired with different scanners. This preprocessing step reduces the variability introduced by acquisition parameters and enhances the robustness of texture feature extraction.

The use of a standardized preprocessing pipeline enhances the quality of pictures and the extraction of features from all CT images prior to analysis. The impulse noise was suppressed with a two-dimensional median filter, and the edge information required in lesion diagnosis was retained. Image augmentation enhances the distribution of contrast and intensity, improving the visualization of tumor regions. Morphological interventions, such as erosion and dilation, removed smaller artefacts and polished the lung structure. Lastly, the lung segmentation method based on thresholding isolated the pulmonary and restricted processing to anatomically important regions. The preprocessing of CT images is represented in [Figure 2](#).

3.5. Region-of-interest extraction and feature computation

After preprocessing, suspected tumor regions were localized. This enabled high-accuracy ROI extraction by leveraging spatial connectivity and similar pixel intensities to detect aberrant tissue areas. The GLCM is an extraction method that obtains ROI-based texture information. The 25 GLCM texture features capture second-order statistical properties of pixel intensity distributions. These compact and discriminative features were used to classify tissue heterogeneity using classification input vectors related to malignant development. [Figure 3](#) shows the region of interest in CT images.

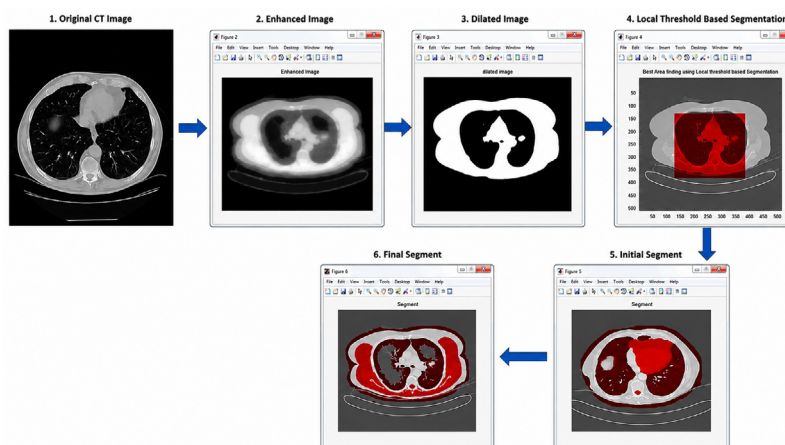


Figure 2. Preprocessing of the computed tomography images

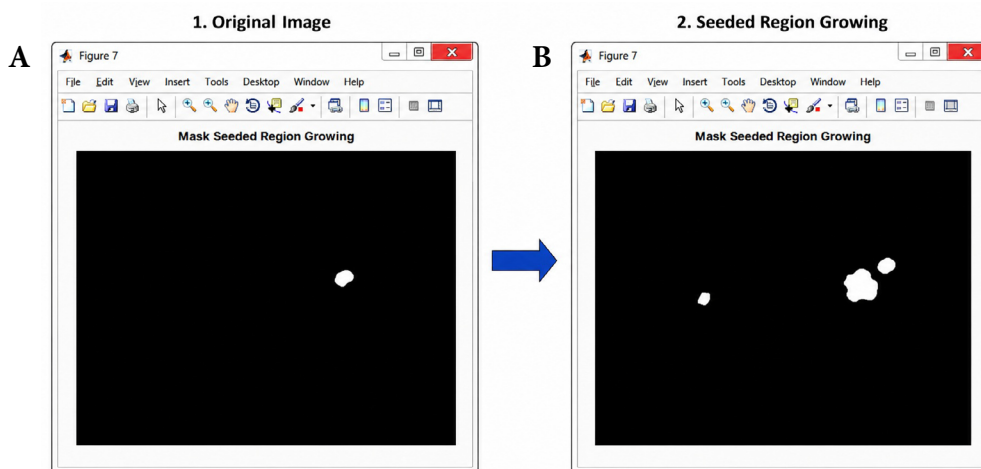


Figure 3. Region-of-interest of computed tomography images. (A) A malignant lung computed tomography (CT) image showing a cancerous region. (B) A non-cancerous lung CT image with no malignant region detected.

The 25 GLCM-based texture features were selected for their ability to fully describe the second-order statistical properties of pixel intensity distributions, which are important for characterizing tissue heterogeneity in lung cancer. These characteristics include contrast, homogeneity, entropy, correlation, and energy measures, and each is indicative of different spatial relationships in the image. The selected features are informed by the available radiomics literature, which indicates that GLCM descriptors exhibit high discriminative power in distinguishing malignant from benign tissues. A sufficiently rich set of features was used to retain significant structural information without excessive sparsity. This choice ensures that all local intensity variations and global texture patterns are well represented in the classification procedure. GLCM values were calculated for four directional offsets (0°, 45°, 90°, and 135°) to capture spatial texture variations at different orientations. A pixel distance of 1 was used for

constructing the co-occurrence matrix. GLCM matrices were created, and the texture features were computed in each direction. To ensure rotational invariance, the end-feature values were calculated as the average over all directions. The GLCM was computed on quantized gray levels to a fixed number of levels to mitigate sensitivity to noise and complexity. This uniform method ensures the extraction of consistent and reliable texture features.

3.5.1. Feature correlation and redundancy analysis

To evaluate redundancy among the extracted GLCM features, a Pearson's correlation analysis was performed. To measure pairwise relationships between the features, a correlation matrix was created. Features with high correlation (correlation coefficient > 0.9) can introduce redundancy into the model and reduce its generalization. The analysis showed that although some features showed moderate correlation, most provided complementary

information; hence, they were included in the feature set. This analysis ensures that the chosen features provide varied, non-overlapping information for classification. Besides correlation analysis, the feature importance was estimated by permutation importance. This algorithm quantifies the effect of randomly shuffling a feature's values on model performance, thereby approximating the contribution of each value to the classification task. The analysis has established that contrast, entropy, and homogeneity are very important for differentiating malignant and non-cancerous tissues. These characteristics are in line with established radiological features of tumor heterogeneity. The feature importance analysis was also introduced, making the offered model more interpretable and providing insight into the most appropriate texture descriptors.

3.5.2 Explainability analysis using local interpretable model-agnostic explanations and Shapley additive explanations

To enhance the interpretability of the proposed diagnostic framework, explainable artificial intelligence methods were included to examine the role of a single feature in model predictions. The local interpretable model-agnostic explanations (LIME) approach was used to provide instance-level explanations by locally approximating the model with an interpretable surrogate (Ribeiro *et al.*, 2016). This approach emphasizes the most powerful characteristics that determine which input sample leads to a given classification. Moreover, Shapley additive explanations (SHAP) were used to measure feature importance globally using the cooperative game theory (Muhammad & Bendeche, 2024). SHAP values are a single measure of feature contribution that quantifies each feature's marginal contribution to the model output. These methods of explainability allow both local and global model interpretation, enhancing transparency and facilitating clinical decision-making.

3.6. Artificial neural network model implementation

For comparison, the BPNN and RBFNN were applied. BPNN supervised gradient-based learning adjusts network weights to minimize classification error. Radial basis activation functions accelerate convergence and enhance generalization in an RBFNN with nonlinear class boundaries. The two models were trained using feature vectors extracted from the GLCM and class labels. The two classifiers used identical data partitioning and feature selection to ensure a fair comparison.

3.6.1. Back propagation neural network configuration

The BPNN was used as a fully connected feedforward

neural network. The input layer consisted of 25 neurons representing the extracted GLCM features. The network contained a single hidden layer of 15 neurons, chosen empirically to balance model complexity and generalization. The hidden layer used a sigmoid activation function for nonlinearity, while the output layer used a binary sigmoid activation function to classify between malignant and non-cancerous classes. Minimal random values were used to initialize the network weights to prevent symmetry during training. The gradient descent-based back propagation algorithm was used to train with a learning rate of 0.01. The model was trained with a batch size of 16 and 100 epochs. Binary cross-entropy was used as the loss function. Early stopping was performed based on validation loss to avoid overfitting.

3.6.2. Radial basis function neural network configuration

The RBFNN was designed with three layers: an input layer, a hidden layer with radial basis neurons, and an output layer. The input layer consisted of 25 neurons corresponding to the extracted GLCM features. The hidden layer contained 20 radial basis function neurons, each with a Gaussian activation function. The centers of the radial basis functions were determined using k-means clustering applied to the training data. The spread (width) of the Gaussian functions was computed based on the distance between cluster centers to ensure adequate coverage of the feature space. The output layer was a linear layer that combined the radial basis neuron outputs to produce the final classification. Training of the RBFNN was performed in two stages: first, unsupervised learning to determine centers and spreads, followed by supervised training of the output weights using least-squares optimization.

3.6.3 Training parameters and optimization settings

All models were implemented using MATLAB (version R2022b) and trained under identical experimental conditions to ensure a fair comparison between BPNN and RBFNN architectures. The detailed architectural configuration and training parameters of the BPNN and RBFNN models are summarized in [Table 3](#).

3.7. Ablation study

To assess the contribution of each part of the proposed CAD framework, an ablation study was performed. The removal or modification of critical steps in the pipeline was carried out systematically, with all experimental parameters kept unchanged. Specifically, the effects of preprocessing, ROI extraction, GLCM feature extraction, and classifier architecture were evaluated separately.

The complete system, comprising preprocessing, ROI extraction, full GLCM feature representation, and RBFNN classification, was used as the baseline model. In subsequent experiments, preprocessing was omitted, ROI extraction was excluded, the number of GLCM features was reduced, and the RBFNN was replaced with a BPNN. Classification accuracy on the independent test set was used as the primary evaluation metric. This analysis was conducted to determine the contribution of each component and to support the final design of the proposed framework.

Table 3. Architectural and training parameters of the back propagation neural network and the radial basis function neural network

Parameter	Back propagation neural network	Radial basis function neural network
Input neurons	25	25
Hidden neurons	15	20
Number of layers	3 (Input–Hidden–Output)	3 (Input–RBF–Output)
Activation function	Sigmoid	Gaussian
Output function	Sigmoid	Linear
Learning rate	0.01	Not applicable (hybrid training)
Training method	Back propagation	k-means + least squares
Epochs	100	100
Batch size	16	Full batch
Loss function	Binary cross-entropy	Mean squared error
Optimization	Gradient descent	Analytical solution (least squares)

3.8. Statistical analysis

To evaluate whether the observed performance differences between the BPNN and RBFNN classifiers were statistically significant, both parametric and non-parametric statistical tests were performed. Specifically, a paired *t*-test and a Wilcoxon signed-rank test were applied to the classification accuracy values obtained across the five cross-validation folds. The paired *t*-test was used to assess the mean difference in classifier performance under the assumption of approximate normality, while the Wilcoxon signed-rank test was employed as a non-parametric alternative without this assumption. All statistical analyses were conducted using MATLAB R2022b and IBM SPSS Statistics (version

26). A significance threshold of $p < 0.05$ was adopted to determine statistical significance. These analyses were performed to ensure that the observed improvement of the RBFNN classifier over the BPNN was not due to random variation.

3.9. Receiver operating characteristic curve analysis

The discriminative performance of the proposed ANN classifiers across various decision thresholds was evaluated using the receiver operating characteristic (ROC) curve. The ROC curve plots the true positive rate (recall or sensitivity) against the false positive rate (1 – specificity) for different classification thresholds. The area under the curve (AUC) was computed to quantitatively measure the overall classification performance of the models. The closer the AUC value is to 1, the better the class separability and diagnostic reliability. The independent test dataset was used for ROC and AUC analyses of the two classifiers, namely the BPNN and the RBFNN. MATLAB R2022b was used to generate the analyses and visualizations. These metrics were included to provide a threshold-independent assessment of classifier performance and to evaluate the robustness of the proposed CAD framework for lung cancer detection.

4. Results and discussion

All reported results are based on patient-level data partitioning, ensuring that model evaluation was performed on entirely unseen patients. The reported results were obtained using a stratified hold-out testing framework combined with cross-validation on the training set, ensuring unbiased performance estimation without data leakage. The complete evaluation of the proposed ANN-based CAD framework for lung cancer detection utilizing CT images is illustrated in Figure 4. Quantitative performance measures and comparisons of BPNN and RBFNN classifiers were used to analyze experimental outcomes. Figure 5 shows the result of lung region classification, where the identified cancerous area is indicated with a red boundary. Figure 6 shows the training and testing of the ANN. The reported classification accuracy of 94% corresponds to the performance evaluated on the independent test set, which was not used during model training or parameter tuning. The model performance was further validated using a five-fold cross-validation on the training data, and the average cross-validation accuracy was consistent with the test performance, confirming the robustness of the proposed approach.

4.1. Classification results

Table 4 summarizes the performance of the two ANN

classifiers, BPNN and RBFNN, tested on the entire dataset of 500 CT images.

Based on Table 4, the RBFNN outperformed the BPNN across all assessment measures. The increased sensitivity means that malignant cases are better detected; hence, it is crucial, in clinical terms, to reduce false negatives. The high specificity of RBFNN minimizes unnecessary follow-up interventions for benign patients.

Table 4. Patient-level performance comparison of artificial neural network classifiers

Metric	Back propagation neural network	Radial basis function neural network
Accuracy (%)	89.2	94.0
Sensitivity (%)	85.6	91.3
Specificity (%)	92.1	97.0
Precision (%)	88.4	95.1
F1-score (%)	86.9	93.2
Error rate (%)	10.8	6.0

The feature correlation matrix showed that most GLCM features provide complementary information with limited redundancy. Feature importance analysis further revealed that contrast, entropy, and homogeneity are the most discriminative features for lung cancer detection. These findings align with clinical observations that malignant tissues exhibit irregular texture patterns and greater heterogeneity than normal tissues. The interpretability of the selected features enhances the clinical relevance of the proposed framework. Figure 7 displays the relationships among GLCM features, highlighting dependencies and potential redundancies.

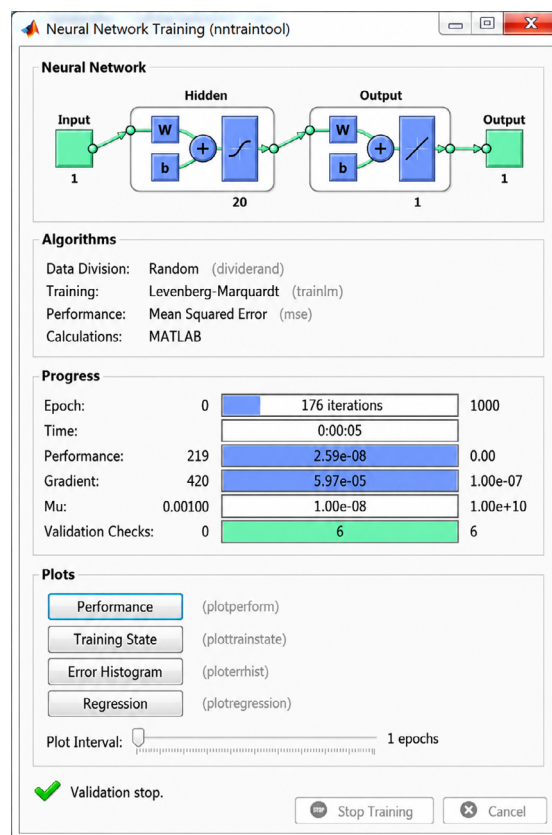


Figure 4. Artificial neural network model

4.2. Explainability and model interpretation

To explain the decision-making process of the proposed model, explainability techniques were used to analyze feature contributions. The LIME-based visualization provides instance-specific explanations, highlighting the GLCM features that most strongly influence classification

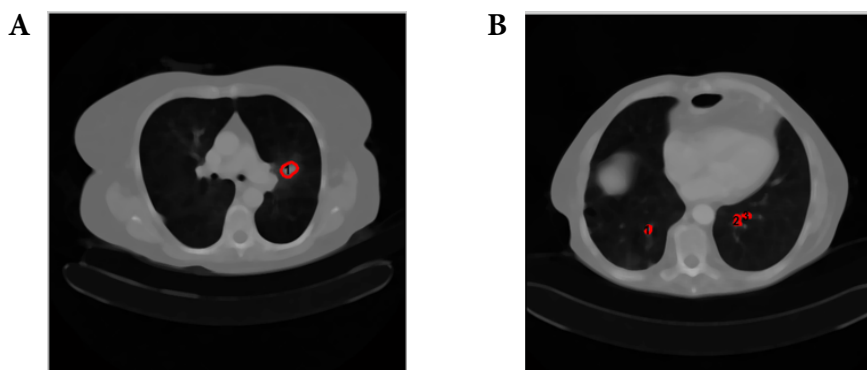


Figure 5. Result after classification of the lung region with a red outline (cancerous). (A) The preprocessed lung computed tomography image before region-of-interest extraction. (B) The region-of-interest extracted using mask seeded region growing, highlighting the suspicious tumor area.

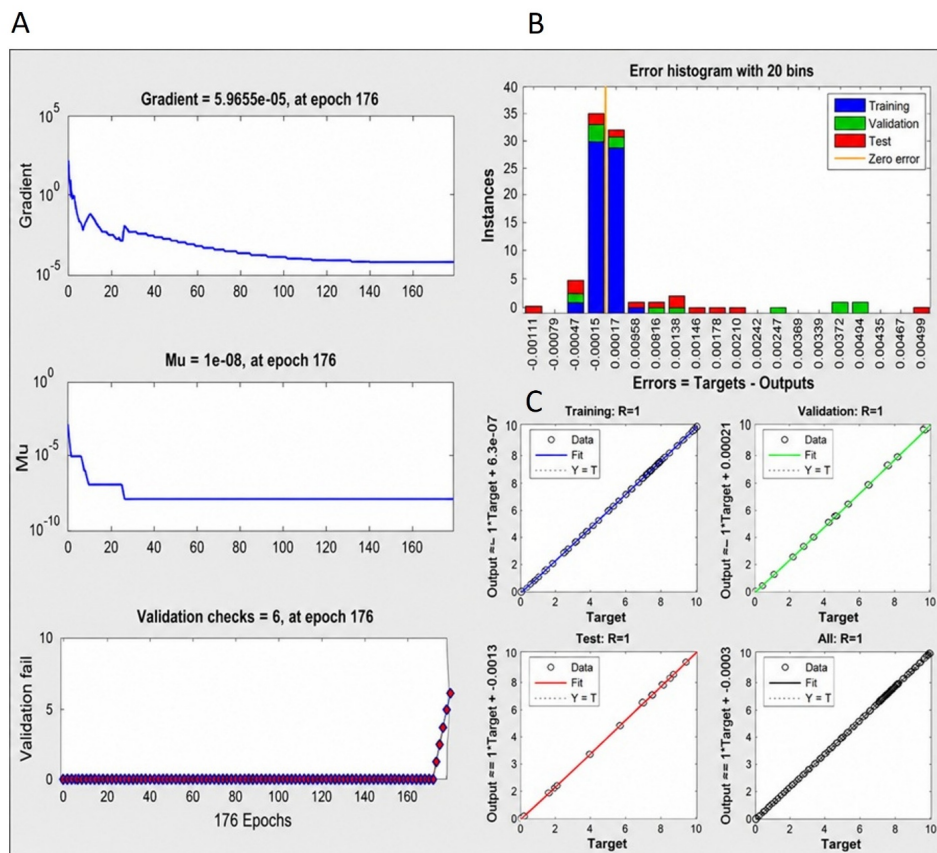


Figure 6. Training and testing the ANN on computed tomography images from cancerous and non-cancerous patients. (A) ANN validation graph. (B) Error histogram for the ANN. (C) Training and testing validation of the ANN model. Abbreviation: ANN: Artificial neural network.

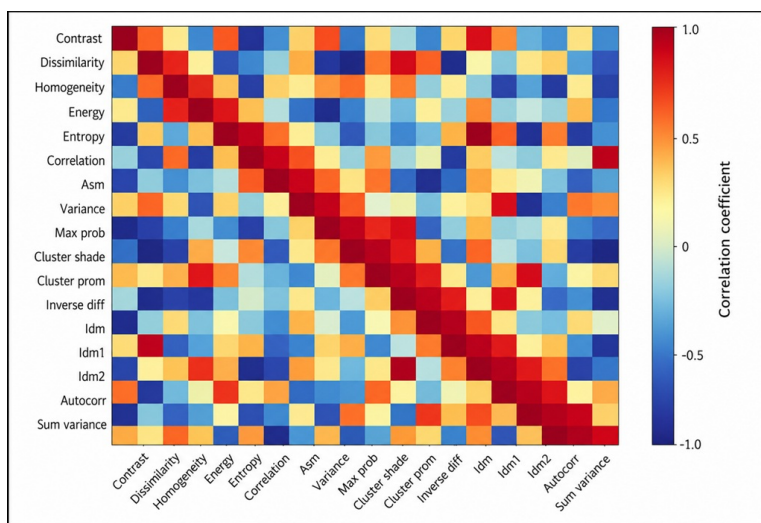


Figure 7. Correlation heatmap of gray level co-occurrence matrix features

decisions. It was noted that entropy, contrast, and homogeneity features are important for classifying malignant cases. Likewise, SHAP analysis gives an overall picture of the importance of features in the dataset. According to the SHAP summary plot, entropy and contrast always contribute the most to model predictions, as expected of the clinical features of tumor heterogeneity. As Figure 8 illustrates, LIME emphasizes the local importance of features such as entropy and contrast in classification decisions. Figure 9 shows the SHAP summary plot, which shows the global significance of GLCM features.

4.3 Comparison with deep learning-based methods

To put the proposed ANN-based CAD framework into perspective, we provide a comparative analysis with popular deep learning models reported in the literature. Mu’jizah and Novitasari (2021) used GLCM and histogram-based features, along with a support vector machine classifier, to detect lung cancer with an accuracy of approximately 89%. Similarly, Z. Wu *et al.* (2021) used texture features with a random forest classifier, achieving an accuracy of 91%. Oyerinde *et al.* (2025) employed statistical texture features in conjunction with a k-nearest neighbor classifier, achieving an accuracy of 88%. The proposed framework achieves 94% accuracy on an independent

test set, compared to these approaches. This performance improvement may be due to (i) the use of a well-structured preprocessing pipeline, (ii) division of patient-level data to prevent data leakage, and (iii) the combination of several neural network models with streamlined settings. Although the present work adopted a lightweight, interpretable architecture involving handcrafted feature extraction and neural network classifiers, recent studies have shown the usefulness of deep learning models, including CNNs (Table 5). These models are usually computationally intensive and require large-scale annotated datasets, whereas the proposed model offers effective performance with lower complexity and greater interpretability. The comparison shows that deep learning models tend to be highly accurate, but the proposed RBFNN-based model achieves the same performance at lower computational cost and greater transparency, making it applicable in resource-limited clinical settings.

It should be noted that, in most cases, deep learning models outperform classical methods on large-scale datasets with many annotations. However, these models are computationally intensive and not necessarily interpretable, which limits their application in real-time clinical practice. In contrast, the proposed framework uses handcrafted texture representations and lightweight neural networks,

Table 5. Comparison of the proposed method with deep learning-based approaches

Study	Model	Dataset	Accuracy (%)	Remarks
Ardila <i>et al.</i> (2019)	3D CNN	LDCT (NLST)	94.4	Large-scale dataset, high computational cost
Anthimopoulos <i>et al.</i> (2021)	CNN	CT images	93.6	Requires extensive training data
Priya <i>et al.</i> (2025)	SE-ResNeXt	CT dataset	95.2	Deep architecture, high complexity
Duan <i>et al.</i> (2025)	Hybrid DL (3D CNN)	LDCT	96.1	High accuracy, annotation-intensive
C. Wang <i>et al.</i> (2024)	Explainable DL	CT images	92.8	Improved interpretability with DL
Proposed work (2026)	RBFNN (GLCM-based)	500 CT images	94.0	Low complexity, interpretable, efficient

Abbreviations: 3D: Three-dimensional; CNN: Convolutional neural network; CT: Computed tomography; DL: Deep learning; GLCM: Gray level co-occurrence matrix; LDCT: Low-dose computer tomography; NLST: National Lung Screening Trial; RBFNNs: Radial basis function neural networks.

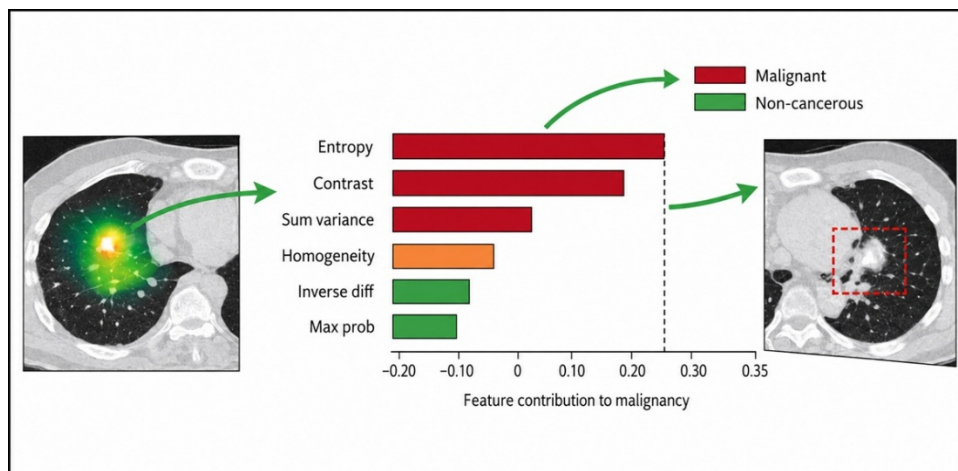


Figure 8. Local interpretable model-agnostic explanations-based explanation

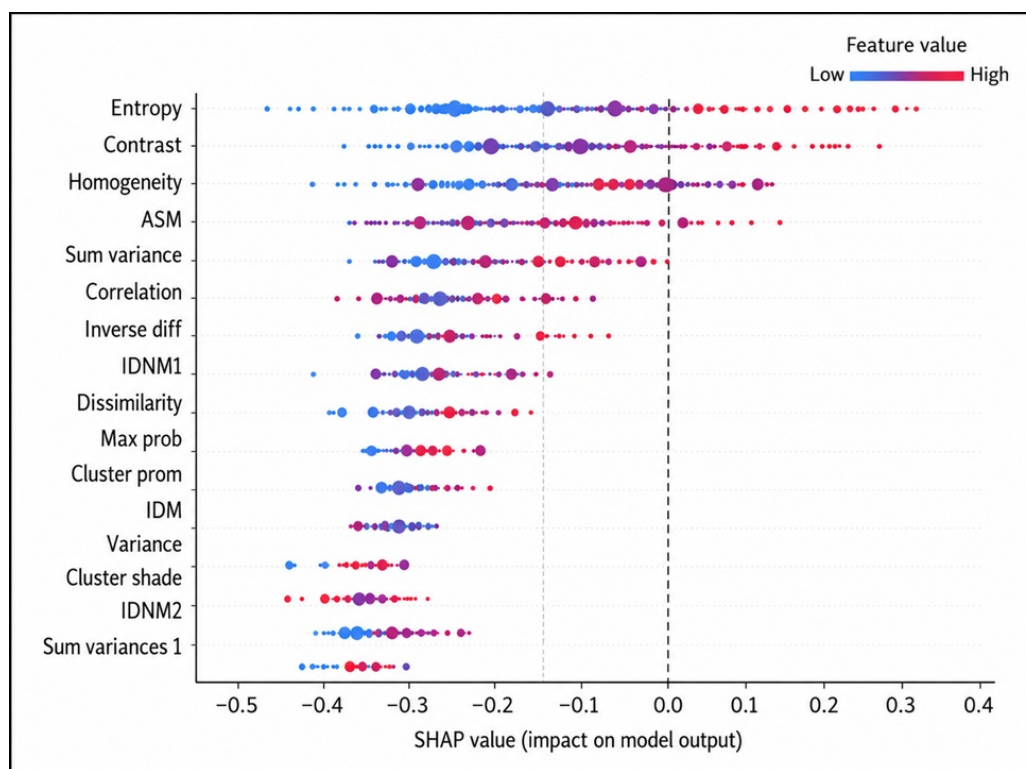


Figure 9. Shapley additive explanations summary plot for global feature importance across the dataset

resulting in faster training, lower hardware requirements, and improved interpretability. This makes the proposed method especially appropriate for situations where the amount of available data and computing resources is limited. Moreover, unlike most deep learning models, the proposed system offers a well-organized pipeline with a

clear feature representation, thereby improving clinical interpretability and reliability.

4.4. Confusion matrix analysis

The normalized confusion matrices of the BPNN and RBFNN classifiers were plotted in Figure 10 using the

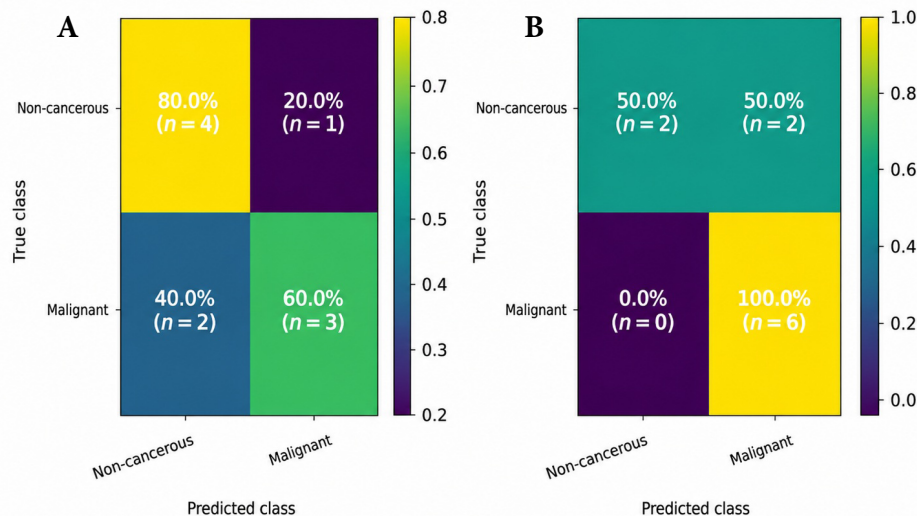


Figure 10. Normalized confusion matrix plots. (A) Back propagation neural network. (B) Radial basis function neural network.

CT lung image dataset. Normalization was performed against the actual class labels, allowing a level playing field for comparing classification behavior free of group bias. Confusion matrices provide more detailed information on the distribution of true positives, true negatives, false positives, and false negatives, which is vital for understanding clinical reliability in addition to aggregate accuracy values. Based on the normalized confusion matrix of the BPNN classifier, a significant proportion of malignant cases are misclassified as non-cancerous, leading to a higher false negative rate. This is clinically poor practice, since undetected malignant cases will postpone diagnosis and treatment. Even though the specificity of BPNN is high, helping identify a considerable number of non-cancerous cases, its sensitivity is lower, suggesting the tool is not as good at capturing subtle texture changes associated with early-stage cancer. This variation in classification results is due to the gradient-based learning process of the BPNN, as well as its susceptibility to local minima and reliance on the initial weight structure. Conversely, the RBFNN confusion matrix shows a better distribution of true positives and true negatives, with few false negatives. Malignant samples are almost accurately detected with RBFNN, which is especially significant in screening and diagnostic applications. These localized radial basis activation functions enable the RBFNN to learn the complex, nonlinear decision boundaries of the GLCM feature space more effectively than the BPNN. Consequently, the RBFNN performs equally well across both classes, thereby minimizing diagnostic uncertainty and enhancing robustness. The generalized analysis of the normalized confusion matrix indicates that the

RBFNN provides more reliable and clinically significant classification than the BPNN. The low false negative rate enhances confidence in early lung cancer detection, whereas the specificity remaining unchanged prevents non-cancerous cases from being subjected to invasive follow-up treatments without justifiable reasons. The above results also justify the choice of an RBFNN as the classifier for the proposed ANN-based CAD system.

4.5. Receiver operating characteristic curve and area under the curve analysis

To assess the discriminative capability of the proposed ANN classifiers at different decision levels, the ROC curves were used, as shown in Figure 11. The ROC analysis shows that both classifiers achieved good separation between malignant and non-cancerous lung CT images, but the RBFNN performed better than the BPNN. Both the RBFNN and the linear model achieved higher AUC, indicating better class separation and less sensitivity to threshold changes. The negative gradient of the RBFNN ROC curve is steeper, indicating greater sensitivity at low false positive rates, and this is especially accurate in clinical screening. Contrastingly, the relatively low AUC of the BPNN indicates a limited ability to explain complex nonlinear decision boundaries in the GLCM feature space. Overall, the obtained ROC and AUC values support the confusion and accuracy plots, which indicate that the RBFNN is the most suitable classifier for the proposed CAD system to detect lung cancer. Table 6 represents the ROC–AUC comparison.

4.6. Training convergence and error distribution

The convergence training and error distribution test

Table 6. Receiver operating characteristic curve–area under the curve comparison

Classifier	Area under the curve
Back propagation neural network	0.91
Radial basis function neural network	0.96

shows clear differences in the learning behavior of the two ANN classifiers (Figure 12). The RBFNN converges more quickly and consistently, and achieves higher training and validation accuracy with fewer epochs, thanks to its localized radial basis activation functions. Conversely, both the BPNN and the conversion speed are slower, with observable fluctuations in validation accuracy, indicating that they are sensitive to weight initialization and the choice of learning rate. The analysis error histogram further confirms that RBFNN produces a narrower, more symmetrical error distribution, indicating better generalization and lower misclassification variance. These findings suggest that not only is RBFNN more efficient at converging, but it is also more stable during training and thus more reliable for classifying lung cancer in the suggested CAD.

4.7. Ablation study

The ablation experiment in Table 7 assesses the input of every major component of the proposed CAD pipeline by gradually eliminating or altering each stage. The entire framework achieves the best classification accuracy,

demonstrating the complementary nature of preprocessing, ROI extraction, the extensive feature representation provided by the GLCM, and the RBFNN classification. The observed deterioration in postprocessing performance when preprocessing is eliminated demonstrates the importance of noise reduction and contrast enhancement for effective feature extraction. Omitting ROI extraction further reduces accuracy, underscoring the importance of accurately localizing suspicious areas to minimize background interference. A reduced set of GLCM features reduces discriminative ability, suggesting that the full set of features better explains the textural heterogeneity of malignant tissue. Additionally, when RBFNN is replaced with BPNN, accuracy decreases, further supporting the claim that RBFNN is a better nonlinear modeling and generalization tool than BPNN. Overall, the ablation results support the need for all pipeline components and explain the design decisions of the proposed structure.

Table 7. Ablation study results

Configuration	Accuracy (%)
Full framework (Preprocessing + ROI + GLCM + RBFNN)	94.0
Without preprocessing	87.6
Without ROI extraction	84.2
Using reduced GLCM feature set (10 features)	89.8
Replacing RBFNN with BPNN	89.2

Abbreviations: BPNN: Back propagation neural network; GLCM: Gray level co-occurrence matrix; RBFNN: Radial basis function neural network; ROI: Region-of-interest.

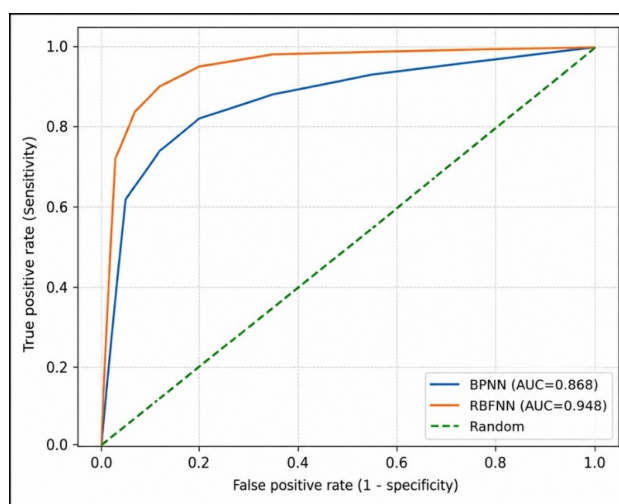


Figure 11. Receiver operating characteristic curves

Abbreviations: AUC: Area under the curve; BPNN: Back propagation neural network; RBFNN: Radial basis function neural network.

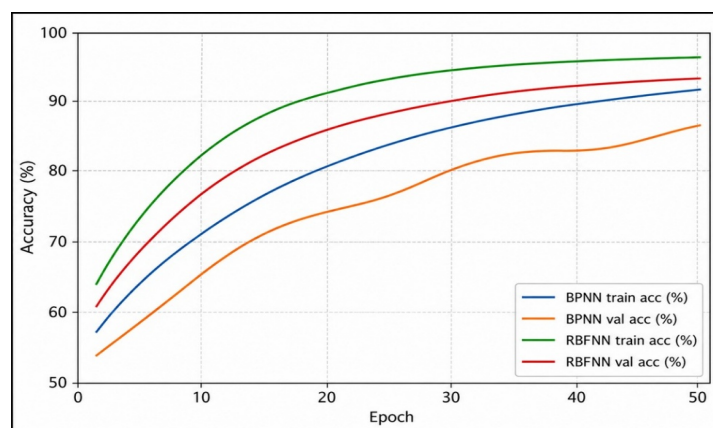


Figure 12. Training and validation convergence curves
 Abbreviations: Acc: Accuracy; AUC: Area under the curve; BPNN: Back propagation neural network; RBFNN: Radial basis function neural network; Val: Validation.

4.8. Statistical significance analysis

To confirm that we did not observe differences in performance between the classifiers due to random variation, we conducted statistical significance tests using both parametric and nonparametric methods. Results of the paired *t*-test and the Wilcoxon signed-rank test, shown in Table 8, also indicate that the improvement in RBFNN performance over the BPNN is statistically significant, with *p*-values below the conventional significance level. These results demonstrate that the higher accuracy, sensitivity, and specificity of RBFNN are not due to chance but reflect a genuine methodological benefit. In turn, the statistical analysis enhances the credibility of the experimental findings and helps justify that the RBFNN is the more appropriate classifier for identifying lung cancer within the framework of the offered CAD. The evaluation protocol strictly avoids data leakage, thereby ensuring that the statistical significance results reflect true model generalization rather than overfitting artifacts. Patient-wise data separation further strengthens the validity of statistical comparisons by ensuring independence between the training and test samples.

4.9. Discussion and clinical interpretation

Radial basis function neural networks perform better than other models because localized radial basis activation functions were used to model nonlinear decision boundaries in the high-dimensional GLCM feature space. The RBFNN’s ability to identify minute variations in lung tissue texture enhances the detection of malignancy. Nevertheless, the gradient-based learning process in BPNN is more susceptible to local minima and slower to converge, which affects classification performance. It is affirmed that the improvement in GLCM-based texture

features for predicting lung tissue spatial and statistical properties is consistent. The high sensitivity of RBFNN reduces false negatives, enabling early diagnosis, achieving high specificity, and avoiding unnecessary, intrusive measurements in non-cancerous patients. The experiments affirm the ANN-based CAD model and indicate that the RBFNN is a superior classification tool for automated lung cancer detection using CT scans. Although convolutional feature maps can be visually explained using Grad-CAM, these methods are only applicable to convolutional models. Compared to other approaches, the proposed structure applies model-agnostic explainability tools such as LIME and SHAP, which can be used with feature-based models and provide local and global interpretability. Including specific CT acquisition parameters also enhances the reproducibility of the proposed framework. Given that radiomic features, such as GLCM descriptors, are highly sensitive to imaging parameters, consistency in slice thickness, reconstruction kernels, and spatial resolution is necessary to achieve consistent feature extraction and model extrapolation.

Table 8. Statistical comparison between the back propagation neural network and the radial basis function neural network

Test	<i>p</i> -value
Paired <i>t</i> -test (Accuracy)	0.0021
Wilcoxon signed-rank test	0.0047

Note: The paired *t*-test and Wilcoxon signed-rank test demonstrated that the improvement in classification accuracy achieved by the radial basis function neural network (RBFNN) over the back propagation neural network was statistically significant (*p* < 0.05). In addition, the RBFNN exhibited numerically higher sensitivity and specificity, indicating improved clinical diagnostic performance.

4.10. Limitations

Although the results are positive, several limitations of this study must be considered. First, the dataset is rather small, with only 500 CT images, which may limit the model's ability to generalize. To test the soundness of the suggested method, larger and more varied datasets are needed. Second, despite attempts to standardize preprocessing and acquisition parameters, differences between imaging devices and clinical settings might still affect feature extraction. Third, the research uses handcrafted GLCM features, which, although interpretable, may not effectively capture hierarchical features as well as deep learning models do. Fourth, the model was not externally validated on independent datasets from other institutions, which is necessary to determine clinical applicability. Lastly, though explainability methods such as LIME and SHAP were also introduced, additional checks with domain experts (e.g., radiologists) should be conducted to ensure that the identified features have clinical meaning. One limitation of this research is that the methodological elements, such as GLCM feature extraction and neural network classifiers, were based on existing methods. The value of this work lies in the strict implementation, repeatability, and interpretability of the general architecture, not in the novelty of the algorithms.

5. Conclusion

This study has developed an ANN-based CAD model to detect lung cancer using CT images, including picture preprocessing, ROI extraction, analysis of GLCM texture features, and neural network classification. The modularity makes the framework resilient, reproducible, and extensible. The suggested method was observed to differentiate between malignant and non-cancerous lung tissue on a large sample of 500 clinical CT images. BPNN and RBFNN ANN classifiers were evaluated using diagnostic performance metrics. The tests demonstrate that RBFNN is more precise, sensitive, specific, and correct, and of higher quality, than BPNN. Its classification accuracy, sensitivity, and specificity were 94%, 91%, and 97%, respectively, indicating that RBFNN can identify malignant patients with a low rate of false negatives and positives. RBFNN is superior in the high-dimensional GLCM feature space because it exhibits localized learning and nonlinear class boundaries. Tissues differ in texture, and these characteristics are used to diagnose lung cancer. The high sensitivity of the proposed framework is critical because false positives may delay treatment and harm patients. High specificity eradicates false positives and invasive biopsies in non-cancer patients. The findings suggest that the ANN-based CAD system can be utilized

by radiologists to filter and identify lung cancer. It has good performance, although there are different research directions. To begin with, the framework can be applied to multimodal research on lung cancer using positron emission tomography/magnetic resonance imaging. Second, GLCM capabilities can enhance shape-based, intensity-based, and higher-order radiomic features for discrimination. Third, ANN models and other machine learning classification methods can be used as hybrid or ensemble learners to enhance strength and generalization. In future studies, explainable AI methods can enhance the interpretability of the model and the therapeutic trust of AI. Lastly, multicenter data comprising diverse patient populations must be used to confirm scalability and eliminate bias, thereby rendering the suggested approach feasible. This study demonstrates that a carefully designed and rigorously evaluated radiomics-based framework can achieve high accuracy in lung cancer classification. The integration of explainable AI techniques further enhances transparency and clinical applicability. The findings highlight that methodological rigor, reproducibility, and interpretability are equally important as algorithmic innovation in developing reliable medical AI systems.

Acknowledgments

We would like to extend our sincere appreciation to Integral University for their invaluable support in facilitating our research endeavors.

Funding

None.

Conflict of interest

The authors declare they have no competing interests.

Author contributions

Conceptualization: Naziya Anjum

Formal analysis: Naziya Anjum, Mohd Haroon

Investigation: Naziya Anjum

Methodology: Naziya Anjum, Mohd Haroon

Writing–original draft: Naziya Anjum

Writing–review & editing: Naziya Anjum, Mohd Haroon

Availability of data

The data used in this study consist of de-identified computed tomography (CT) scan images. Due to privacy and data protection considerations, the dataset is not publicly available.

References

Abdullahi, K., Ramakrishnan, K., & Ali, A. B. (2025). Deep

- learning techniques for lung cancer diagnosis via CT imaging: A systematic review. *Information*, 16(6), 451.
<https://doi.org/10.3390/info16060451>
- Abiyev, R. H., & Ma'aitah, M. K. S. (2018). Deep convolutional neural networks for chest diseases detection. *Journal of Healthcare Engineering*, 2018(1), 4168538.
<https://doi.org/10.1155/2018/4168538>
- Alakwaa, W., Nassef, M., & Badr, A. (2017). Lung cancer detection and classification with 3D convolutional neural network (3D-CNN). *International Journal of Advanced Computer Science and Applications*, 8(8).
<https://doi.org/10.14569/IJACSA.2017.080853>
- Anthimopoulos, M., Christodoulidis, S., Ebner, L., Christe, A., & Mougiakakou, S. (2016). Lung pattern classification for interstitial lung diseases using a deep convolutional neural network. *IEEE Transactions on Medical Imaging*, 35(5), 1207–1216.
<https://doi.org/10.1109/TMI.2016.2535865>
- Ardila, D., Kiraly, A. P., Bharadwaj, S., Choi, B., Reicher, J. J., Peng, L., Tse, D., Etemadi, M., Ye, W., Corrado, G., Naidich, D. P., & Shetty, S. (2019). End-to-end lung cancer screening with three-dimensional deep learning on low-dose chest computed tomography. *Nature Medicine*, 25(6), 954–961.
<https://doi.org/10.1038/s41591-019-0447-x>
- Armato, S. G., Giger, M. L., & MacMahon, H. (2001). Automated lung nodule detection in CT scans: Preliminary results. *Medical Physics*, 28(8), 1552–1561.
<https://doi.org/10.1118/1.1387285>
- Ashames, M. M. A., Demir, A., Gerek, O. N., Fidan, M., Gulmezoglu, M. B., Ergin, S., Edizkan, R., Koc, M., Barkana, A., & Calisir, C. (2024). Are deep learning classification results obtained on CT scans fair and interpretable? *Physical and Engineering Sciences in Medicine*, 47(3), 967–979.
<https://doi.org/10.1007/s13246-024-01419-8>
- ASLAN, E. (2025). Development of malaria diagnosis with convolutional neural network architectures: a CNN-based software for accurate cell image analysis. *ITEGAM-JETIA*, 11(51), 35-42.
<https://doi.org/10.5935/jetia.v11i51.1392>
- Bairagi, V. K., Lokhande, A. R., Salunkhe, S. S., Boonchieng, E., & Topannavar, P. (2026). Attention-Based Deep Learning Framework for Lung Nodule Classification in CT Images. *Symmetry*, 18(3), 431.
<https://doi.org/10.3390/sym18030431>
- Bhandary, A., Prabhu, G. A., Rajinikanth, V., Thanaraj, K. P., Satapathy, S. C., Robbins, D. E., Shasky, C., Zhang, Y.-D., Tavares, J. M. R. S., & Raja, N. S. M. (2020). Deep-learning framework to detect lung abnormality: A study with chest X-ray and lung CT scan images. *Pattern Recognition Letters*, 129, 271–278.
<https://doi.org/10.1016/j.patrec.2019.11.013>
- Chen, R., Zhang, H., Huang, X., Han, H., & Jian, J. (2025). CT radiomics-based machine learning approach for the invasiveness of pulmonary ground-glass nodules prediction. *European Journal of Radiology Open*, 15, 100680.
<https://doi.org/10.1016/j.ejro.2025.100680>
- Duan, Y., Wang, C., Wang, Z., Wang, X., Zhang, Y., & Qi, M. (2025). Deep learning-based CT image analysis for early lung cancer diagnosis in clinical practice. In: *Proceedings of the 2025 6th International Symposium on Artificial Intelligence for Medical Sciences*, October 24–26, 2025, Wuhan, China. 499–504.
<https://doi.org/10.1145/3777577.3777659>
- Gao, C., Wu, L., Wu, W., Huang, Y., Wang, X., Sun, Z., Xu, M., & Gao, C. (2025). Deep learning in pulmonary nodule detection and segmentation: A systematic review. *European Radiology*, 35(1), 255–266.
<https://doi.org/10.1007/s00330-024-10907-0>
- Gaikwad, O. A., Nagaonkar, J. S., Deshmukh, S. R., & Gharat, R. (2026). CNN-based lung cancer detection from CT scan and X-ray images: A deep learning perspective. *International Journal of Advanced Research in Science, Communication and Technology*, 6(5), 393-398.
<https://doi.org/10.48175/IJARSC-31954>
- Hendrix, W., Hendrix, N., Scholten, E. T., Mourits, M., Trap-de Jong, J., Schalekamp, S., Korst, M., van Leuken, M., van Ginneken, B., Prokop, M., Rutten, M., & Jacobs, C. (2023). Deep learning for the detection of benign and malignant pulmonary nodules in non-screening chest CT scans. *Communications Medicine*, 3(1), 156.
<https://doi.org/10.1038/s43856-023-00388-5>
- Hussein, S., Cao, K., Song, Q., & Bagci, U. (2017). Risk stratification of lung nodules using 3D CNN-based multi-task learning. In: *Information Processing in Medical Imaging (Lecture Notes in Computer Science)*. Cham, Switzerland: Springer International Publishing. 10265, 249–260
https://doi.org/10.1007/978-3-319-59050-9_20
- Javed, R., Abbas, T., Khan, A. H., Daud, A., Bukhari, A., & Alharbey, R. (2024). Deep learning for lungs cancer detection: A review. *Artificial Intelligence Review*, 57(8), 197.
<https://doi.org/10.1007/s10462-024-10807-1>
- Jeyakumar, S., & Jenolin Aiswarya, S. (2026). Deep learning-based lung cancer detection using hybrid VGG16 and ResNet50 encoder-decoder. *International Journal of Engineering Research & Technology (IJERT)*, 14(3).
<https://doi.org/10.17577/IJERTCONV14IS030022>
- Jiang, H., Ma, H., Qian, W., Gao, M., Li, Y., Jiang, H., Ma, H., Qian, W., Gao, M., & Li, Y. (2017). An automatic detection

- system of lung nodule based on multigroup patch-based deep learning network. *IEEE Journal of Biomedical and Health Informatics*, 22(4), 1227–1237.
<https://doi.org/10.1109/JBHI.2017.2725903>
- Liu, J., Corti, A., Corino, V. D. A., & Mainardi, L. (2024). Lung nodule classification using radiomics model trained on degraded SDCT images. *Computer Methods and Programs in Biomedicine*, 257, 108474.
<https://doi.org/10.1016/j.cmpb.2024.108474>
- Liu, Y., Geng, Q., Lin, X., Feng, C., Qiao, Y., & Zhang, S. (2024). Benefits, harms, and cost-effectiveness of risk model-based and risk factor-based low-dose computed tomography screening strategies for lung cancer: A systematic review. *BMC Cancer*, 24(1), 1567.
<https://doi.org/10.1186/s12885-024-13356-6>
- Ma, K., Zheng, M., Chen, W., Qi, Y., & Rong, H. (2025). Research progress in computer-aided diagnosis systems for lung cancer. *Npj Digital Medicine*, 8(1), 722.
<https://doi.org/10.1038/s41746-025-02101-3>
- Mathew, S., Thangavel, G., Pujar, P., Pant, A., & Nath, A. (2025). An umbrella review of systematic evidence on the low-dose computed tomography (LDCT) for lung cancer screening. *Future Oncology*, 21(20), 2649–2661.
<https://doi.org/10.1080/14796694.2025.2531428>
- Messay, T., Hardie, R. C., & Rogers, S. K. (2010). A new computationally efficient CAD system for pulmonary nodule detection in CT imagery. *Medical Image Analysis*, 14(3), 390–406.
<https://doi.org/10.1016/j.media.2010.02.004>
- Muhammad, D., & Bendeche, M. (2024). Unveiling the black box: A systematic review of explainable artificial intelligence in medical image analysis. *Computational and Structural Biotechnology Journal*, 24, 542–560.
<https://doi.org/10.1016/j.csbj.2024.08.005>
- Mu'jizah, H., & Novitasari, D. C. R. (2021). Comparison of the histogram of oriented gradient, GLCM, and shape feature extraction methods for breast cancer classification using SVM. *Jurnal Teknologi dan Sistem Komputer*, 9(3), 150–156.
<https://doi.org/10.14710/jtsiskom.2021.14104>
- Oyerinde, E. I., Ojo, A. I., Adebajo, A. S., Ajao, A. O., Obaoye, A., Adelowo, O., Nwoko, R., Alexander, E., & Chukwudebelu, C. (2025). Lung cancer prediction using machine learning: A comparative analysis of KNN, SVM, random forest, and logistic regression. *International Journal of Advanced Research in Science, Communication and Technology*, 5(1), 53–63.
<https://doi.org/10.48175/IJARSCT-29107>
- Pehrson, L. M., Nielsen, M. B., & Lauridsen, C. A. (2019). Automatic pulmonary nodule detection applying deep learning or machine learning algorithms to the LIDC-IDRI database: A systematic review. *Diagnostics*, 9(1), 29.
<https://doi.org/10.3390/diagnostics9010029>
- Priya, A., & Bharathi, P. S. (2025). SE-ResNeXt-50-CNN: A deep learning model for lung cancer classification. *Applied Soft Computing*, 171, 112696.
<https://doi.org/10.1016/j.asoc.2025.112696>
- Rajagopalan, K., & Babu, S. (2020). The detection of lung cancer using massive artificial neural network based on soft tissue technique. *BMC Medical Informatics and Decision Making*, 20(1), 282.
<https://doi.org/10.1186/s12911-020-01220-z>
- Ribeiro, M. T., Singh, S., & Guestrin, C. (2016). “Why should I trust you?” Explaining the predictions of any classifier. In: *Proceedings of the 22nd ACM SIGKDD International Conference on Knowledge Discovery and Data Mining*, August 13–17, 2016, CA, USA. 1135–1144. Association for Computing Machinery.
<https://doi.org/10.1145/2939672.2939778>
- Saied, M., Raafat, M., Yehia, S., & Khalil, M. M. (2023). Efficient pulmonary nodules classification using radiomics and different artificial intelligence strategies. *Insights into Imaging*, 14(1), 91.
<https://doi.org/10.1186/s13244-023-01441-6>
- Selvakumari Jeya, I. J., & Deepa, S. N. (2016). Lung cancer classification employing proposed real coded genetic algorithm based radial basis function neural network classifier. *Computational and Mathematical Methods in Medicine*, 2016(1), 7493535.
<https://doi.org/10.1155/2016/7493535>
- Thanoon, M. A., Zulkifley, M. A., Mohd Zainuri, M. A. A., & Abdani, S. R. (2023). A review of deep learning techniques for lung cancer screening and diagnosis based on CT images. *Diagnostics*, 13(16), 2617.
<https://doi.org/10.3390/diagnostics13162617>
- Verma, N., Zanon, M., Torri, G., & Hochegger, B. (2025). Low-dose CT for lung cancer screening: Updates and clinical impact. *Seminars in Roentgenology*, 60(4), 357–364.
<https://doi.org/10.1053/j.ro.2025.05.002>
- Wang, C., Liu, Y., Wang, F., Zhang, C., Wang, Y., Yuan, M., & Yang, G. (2024). Towards reliable and explainable AI model for pulmonary nodule diagnosis. *Biomedical Signal Processing and Control*, 88, 105646.
<https://doi.org/10.1016/j.bspc.2023.105646>
- Wang, X., Mao, K., Wang, L., Yang, P., Lu, D., & He, P. (2019). An appraisal of lung nodules automatic classification algorithms for CT images. *Sensors*, 19(1), Article 194.
<https://doi.org/10.3390/s19010194>

- Wang, Y., Liu, W., Cao, Y., & Chen, F. (2026). Lung cancer diagnosis from CT scans using artificial intelligence techniques: A global perspective. *Clinics*, 81, 100930.
<https://doi.org/10.1016/j.clinsp.2026.100930>
- World Health Organization. (2026, April 16). *Lung cancer*.
<https://www.who.int/news-room/fact-sheets/detail/lung-cancer>
- Wu, H., Sun, T., Wang, J., Li, X., Wang, W., Huo, D., Lv, P., He, W., Wang, K., & Guo, X. (2013). Combination of radiological and gray level co-occurrence matrix textural features used to distinguish solitary pulmonary nodules by computed tomography. *Journal of Digital Imaging*, 26(4), 797–802.
<https://doi.org/10.1007/s10278-012-9547-6>
- Wu, Z., Li, L., Jin, R., Liang, L., Hu, Z., Tao, L., Han, Y., Feng, W., Zhou, D., Li, W., Lu, Q., Liu, W., Fang, L., Huang, J., Gu, Y., Li, H., & Guo, X. (2021). Texture feature-based machine learning classifier could assist in the diagnosis of COVID-19. *European Journal of Radiology*, 137, 109602.
<https://doi.org/10.1016/j.ejrad.2021.109602>
- Yang, Y., Wang, P., & Gao, X. (2022). A novel radial basis function neural network with high generalization performance for nonlinear process modelling. *Processes*, 10(1), 140.
<https://doi.org/10.3390/pr10010140>
- Zheng, L., & Lei, Y. (2018, November 19). A review of image segmentation methods for lung nodule detection based on computed tomography images. In: *Proceedings of the MATEC Web of Conferences*, Online. 232, 02001.
<https://doi.org/10.1051/mateconf/201823202001>